JOURNAL OF GEOPHYSICAL RESEARCH, VOL. 112, C05034, doi:10.1029/2004JC002716, 2007

An unexpected seasonal variability of salinity in the Beaufort Sea upper layer in 1996–1998

Jiayan Yang[1] and Josefino C. Comiso[2]

Received 15 September 2004; revised 29 September 2006; accepted 3 January 2007; published 17 May 2007.

[1] The salinity in the upper Beaufort Sea from the mixed layer to the thermocline layer was observed by drifting buoys from 1996 to 1998. The salinity in this depth range was lower in winter and higher in the summer, the exact opposite from what one would expect from the seasonal cycle of the freshwater flux associated with the ice melting/freezing and river runoff. In this study, we calculated the daily Ekman transport and upwelling velocity in the Beaufort Sea, using both satellite and buoy data. In fall and winter months, the offshore transport of low-salinity water from the coastal area toward the interior where the buoys were located was observed to be strong. This horizontal Ekman transport led to the freshening of the surface Ekman layer in the buoy location. The convergence of the Ekman transport resulted in a strong downwelling in the offshore regions, and so the halocline and thermocline were pushed downward. The downwelling then results in the freshening of the subsurface salinity as observed by buoys. Other processes, such as lateral advection, may have also played a role in the subsurface freshening. The lack of in situ observations needed to estimate the salinity gradient makes it difficult to assess more accurately the contribution from lateral advection. A scaling analysis using the salinity climatology suggests that the lateral salinity advection, though considerably smaller than the vertical one, may not be negligible.

Citation: Yang, J., and J. C. Comiso (2007), An unexpected seasonal variability of salinity in the Beaufort Sea upper layer in 1996–1998, *J. Geophys. Res.*, *112*, C05034, doi:10.1029/2004JC002716.

1. Introduction

[2] The seasonal salinity variation of the upper Arctic Ocean is strongly influenced by the annual freezing and melting cycle of sea ice. Brine rejection during ice formation in autumn and winter leads to higher salinity, whereas freshwater flux due to melting ice in spring and summer results in a fresher upper ocean. River runoff, which also reaches its maximum rate in spring and summer, further enhances this hydrologic cycle in the Arctic Basin. On the basis of the seasonal cycle of the freshwater input, it is expected that salinity in the upper Arctic Ocean would increase from later summer or early fall, when the sea-ice coverage is minimum, to the late winter or early spring, when the sea-ice volume reaches its maximum. Actual observations, however, have been shown to be inconsistent with this expected seasonal cycle of the salinity. An example of such observations was that collected by the Ice-Ocean Environmental Buoys (IOEB), deployed jointly by Woods Hole Oceanographic Institution (WHOI) and Japan Marine Science and Technology Center (JAMSTEC) in Beaufort Sea in 1990s [*Honjo et al.*, 1995]. *Comiso et al.* [2003] analyzed the upper ocean temperature and salinity data from such autonomous buoys deployed in the Beaufort Sea and found out that for the 1996–1998 period, when hydrographic data were available, the salinity was maximum in the summer and minimum in the winter season (see Figures 14–17 of Comiso et al.'s paper).

[3] As will be shown later, the sea-ice cover near the buoy and vicinity went through very similar cycles of winter freezing and summer melting in all 3 years. Intuitively, the observed seasonal variation in salinity cannot be explained by the freshwater flux and must be caused by internal oceanic processes. The spatial variation of salinity along the buoy trajectories, as to be discussed, does not explain the magnitudes of freshening in the winter months. We hypothesize that the oceanic advection plays a leading role in the observed seasonal salinity variability. In this paper, we will analyze data of sea-ice motion, surface geostrophic wind, and sea-ice concentration for the 4-year period from 1995 to 1998 to generate daily basin-wind surface stress field. The upwelling and downwelling field will be calculated by estimating the divergence of the Ekman layer transport and will be used to gain insights into the unexpected phenomenon.

2. The Seasonal Variability of Salinity in the Beaufort Sea

[4] The salinity data shown here were from drifting IOEB platforms in the Beaufort Sea in 1996, 1997, and 1998. The

[1]Department of Physical Oceanography, Woods Hole Oceanographic Institution, Woods Hole, Massachusetts, USA.
[2]Laboratory for Hydrospheric and Biospheric Sciences, NASA Goddard Space Flight Center, Greenbelt, Maryland, USA.

0148-0227/07/2004JC002716$09.00

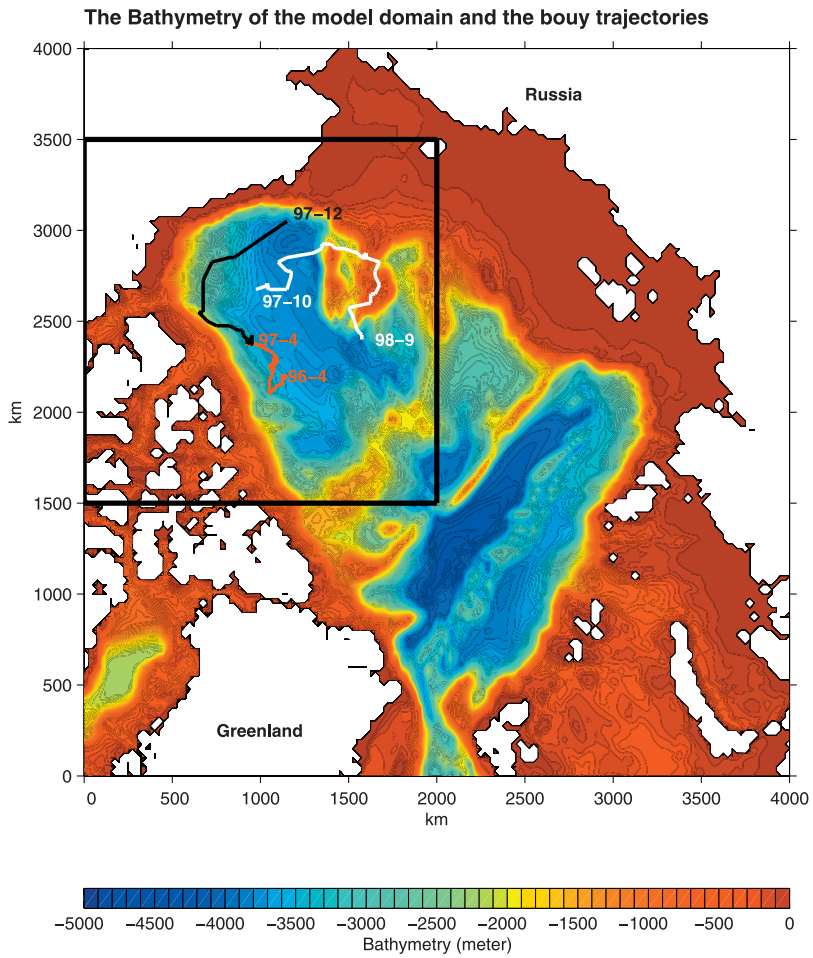

Figure 1. Arctic bathymetry and the buoy trajectory (red line is for B96 IOEB between April 1996 and April 1997, black line for B97 IOEB between April 1997 and December 1997, and white line for the SHEBA IOEB between October 1997 and September 1998). The black box is the area that this study will be focused on. Note that for a 1-year period, the B96 moved only over a relatively short distance (red line).

IOEB was designed to acquire a comprehensive set of environmental data while drifting in the Arctic pack ice through all seasons for several years [*Krishfield*, 1999]. An IOEB was initially deployed in the Beaufort Sea in 1992 (referred to as the Beaufort IOEB hereafter). It had been refurbished several times over a 6-year period between 1992 and 1998. The hydrographic data were available only after the refurbishment in April 1996. The buoy was refurbished again in April 1997 and continued to drift until it was trapped in the shelf area in early 1998. So only the salinity data for the period between April 1996 and December 1997 could be used for this study. The trajectory of the buoy is shown in Figure 1. The red line indicates the trajectory between two refurbishments in April of 1996 and 1997, and the black line indicates the period after the second refurbishment. It is interesting to note that the Beaufort IOEB was nearly stagnant, moving only about 250 km, over the entire 12 months between two refurbishments (red line in Figure 1). Another buoy, Surface Heat Budget of the Arctic Ocean (SHEBA) IOEB, was deployed on 30 September 1997 in the Beaufort Sea. The salinity was measured at 65, 105, and 165 m. The trajectory of the SHEBA IOEB is shown by the white line in Figure 1. The oceanic changes within the black box, shown in Figure 1, will be the focus of this study.

[5] The temperature and salinity variations from all IOEB buoys have been analyzed in previous studies [e.g., *Honjo et al.*, 1995; *Comiso et al.*, 2003; *Yang et al.*, 2004]. The specific feature that this study will address is the unexpected seasonal variation of salinity reported by *Comiso et al.* [2003]. For instance, Figure 2 shows the temperature-salinity diagram for the salinity variation between April 1996 and December 1997 at the depth of 45 m. The gray dots correspond to all data available during this period, and the black dots in each box indicate the T-S values in that particular month. During this 20-month period, the salinity was highest in August 1996 and August 1997, and lowest in December 1996, January 1997, and November 1997. Similar patterns were found at 8 and at 76 m from the Beaufort IOEB data. The other buoy, i.e., the SHEBA IOEB, measured temperature and salinity at greater depths from 65 to 165 m. The monthly T-S diagram at 65 m, again from Comiso et al.'s paper, is shown in Figure 3. In the 1-year period from October 1997 to September 1998, the

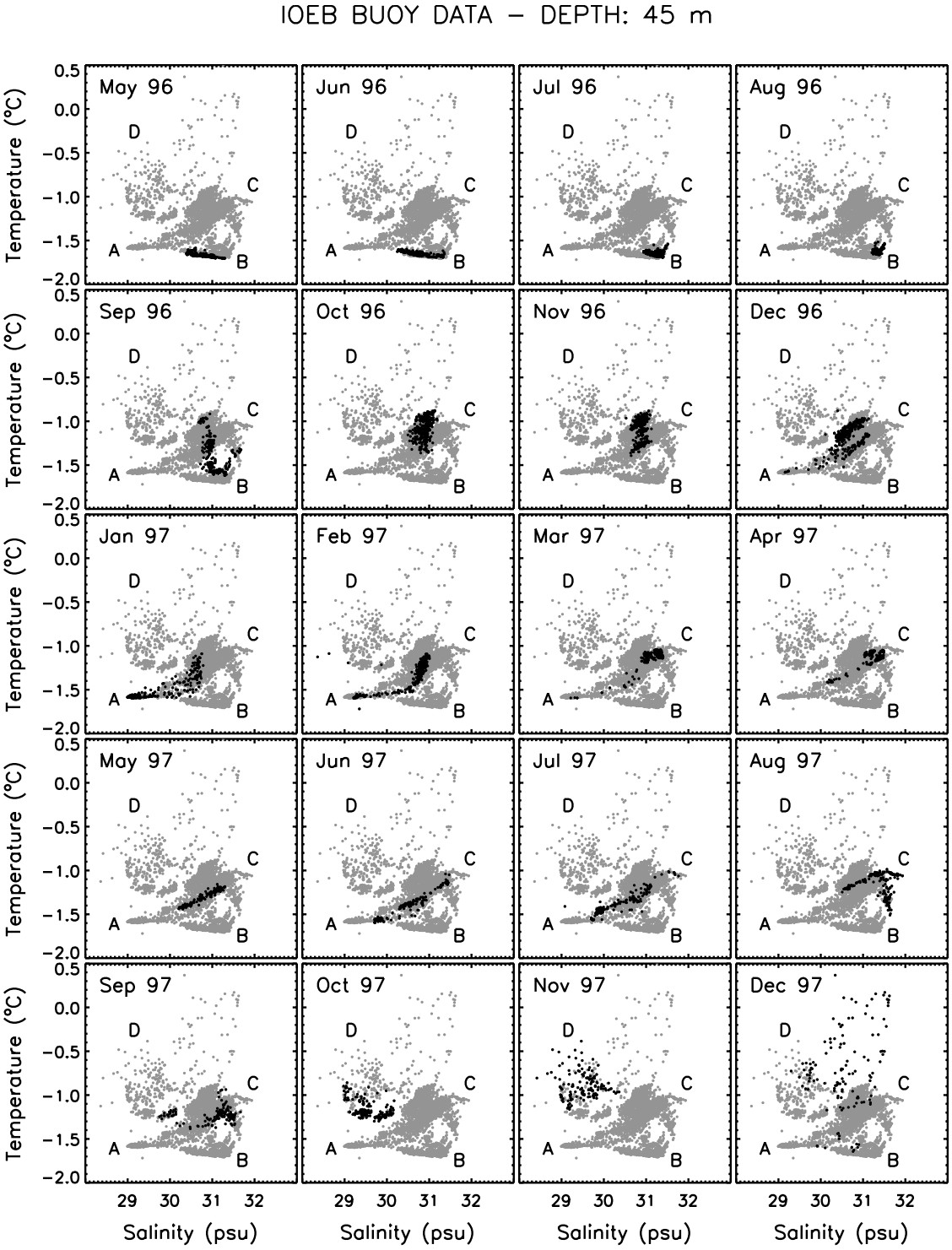

Figure 2. T-S diagram of daily temperature and salinity during each month (in black dots) at 45 m observed by B96 and B97 buoys. The gray dots correspond to all available data at this depth over the period from April 1996 to December 1997 (from *Comiso et al.* [2003]).

salinity was generally lower in the winter and higher in the summer. The minimum salinity was observed in December and January, and the highest one was in June-September period. Similar patterns were found in T-S diagrams at different depths [see *Comiso et al.*, 2003].

[6] What can be possibly responsible to this unexpected seasonal cycle in the Beaufort Sea? A possible explanation is that the changes were merely due to the spatial variations along the buoy trajectories. The Beaufort IOEB buoy drifted only about 150 km between August 1996 and January 1997 [*Krishfield*, 1999]. The salinity change over this period was

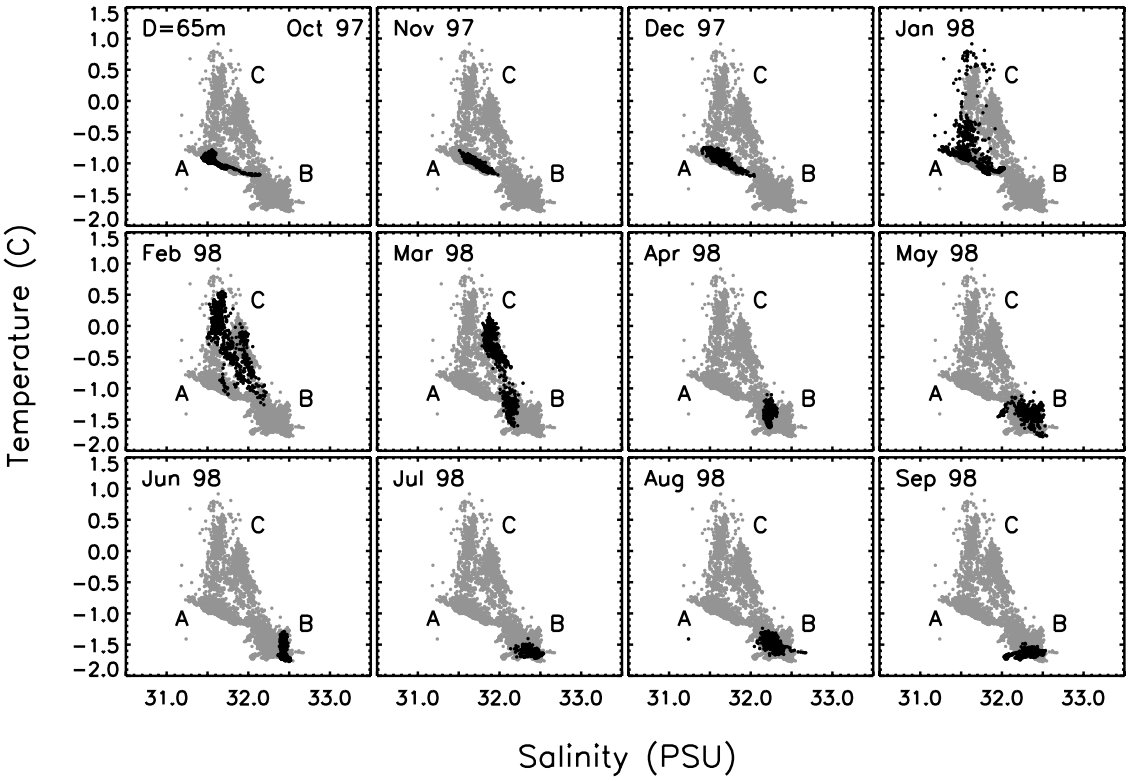

Figure 3. T-S diagram for daily temperature and salinity data at 65 m from SHEBA IOEB buoy (from *Comiso et al.* [2003]).

over 1 psu at the 45-m depth (Figure 2). Without sufficient salinity data at this depth in this time period, it would be difficult to quantify how much of the observed difference was due to the spatial variation of salinity. Nevertheless, we have used the annual-mean salinity data from the Polar Science Center's Hydrography Climatology (PHC) [*Steele et al.*, 2001] at the 50-m depth. The spatial variation of salinity was within 0.2 psu during the whole 12 months between two refurbishments (April 1996 and 1997). The buoy was indeed located in a slightly higher salinity region in August 1996 than in January 1997. It is possible that the PHC climatology is too smooth, and the real spatial variation was actually greater in 1996 and 1997. But such spatial changes would be unlikely to account for the reduction of 1 psu from August 1996 to January 1997 over a distance of 150 km. It is thus more likely that physical processes may have played a leading role in the observed phenomenon. The upper ocean salinity is affected by several processes. The seasonal melting and freezing cycle and the river runoff are two major sources of freshwater fluxes. If the salinity variations were forced by these fluxes, one would expect that salinity be higher in the winter than in the summer, the opposite of what were shown in Figures 2 and 3. Another process that could cause an increase in salinity is brine drainage which occurs through gravitation and thereby leads to the release of the salty solution to the underlying seawater. However, the salinity of sea ice, even the first year ice, is typically much lower than that of seawater. During the summer melt, the dilution of low salinity water with surface water underneath the ice is likely a much more dominant process than brine drainage, especially in predominantly multiyear ice region (i.e., where the IOEBs were located) where the salinity of the ice floes are already close to zero. A further possibility would be the vertical mixing induced by brine rejection in the winter. The static instability occurs when the salinity in the mixed layer becomes higher than that in the subsurface (the density is determined almost solely by the salinity since the water temperature is nearly uniformly at the freezing point in the mixed and halocline layers). If this happened, the salinity in the subsurface layer would increase (for example, at 45-m depth in the winter months), but this would be in contradiction to the IOEB observed changes. Another type of mixing is forced by intense stirring associated with the occurrences of storms. The role of storm-induced mixing in the IOEB-observed variations has been examined by *Yang et al.* [2004] and would not be able to explain this peculiar seasonal cycle. A clear indication of a storm-induced mixing, which typically occurs on the timescale of a few days [*Yang et al.*, 2004], is the homogenization of the whole water column within the mixed layer. Salinity in the surface layer could increase dramatically during the storm, and this phenomenon had been observed in different seasons by IOEBs. The salinity change described in this study is gradual evolution on the annual time. This characteristic indicates that the storm-induced mixing, which is sporadic in nature, was not responsible for the seasonal changes that we are investigating here.

[7] The remaining process that can have a major impact on salinity is the advection, both horizontal and vertical. A prominent feature of the Arctic Ocean is the presence of a shallow halocline which is just about 35–80 m below the

surface in this region during the IOEB period as the data from CTD (conductivity, temperature, and depth) stations made during the two refurbishments show [*Comiso et al.*, 2003]. Salinity in this depth range is thus very sensitive to the vertical movement of the halocline layer. In the following, we will discuss how the Ekman transport and pumping contribute to the seasonal changes of salinity in the region of IOEB deployments.

3. Data and Model

[8] Surface stress data are used to calculate the Ekman transport. The Arctic Ocean Ekman layer is forced by wind stress directly in the open-water areas and indirectly in the ice-covered areas. To partition the air-water and ice-water stresses in each model grid, we used the daily sea-ice concentration data with a spatial resolution of 25 km provided by satellite passive microwave sensors continuously in the last 26 years [*Comiso*, 1995]. The total stress in each grid is calculated by:

$$\vec{\tau} = \alpha \vec{\tau}_{\text{ice-water}} + (1-\alpha)\vec{\tau}_{\text{air-water}} \tag{1}$$

where α is the fraction of the grid that is covered by sea ice, and $\vec{\tau}_{\text{ice-water}}$ and $\vec{\tau}_{\text{air-water}}$ are the ice-water and air-water interfacial stresses, respectively. The sea-ice concentration data are used to calculate α.

[9] The surface wind vector is needed for calculating the air-water stress. In this study, we follow the procedure that has been adopted by the Arctic Ocean Model Intercomparison Project (AOMIP) [*Proshutinsky et al.*, 2001]. The sea-level pressure (SLP) data are used to calculate the surface geostrophic wind which is then converted to a 10-m surface wind by an empirical formula [*Proshutinsky and Johnson*, 1987]. In the study, the twice daily SLP data from the International Arctic Buoy Program (IABP) [*Rigor*, 2002] are interpolated into the 25-km model grid. The geostrophic wind vector, (u_g, v_g), is then computed from this regridded SLP data. Following the AOMIP procedure, the 10-m surface wind vector is computed by using the following equations:

$$\begin{aligned} u_s &= 0.8\left(u_g \cos 30^\circ - v_g \sin 30^\circ\right) \\ v_s &= 0.8\left(u_g \cos 30^\circ + v_g \sin 30^\circ\right) \end{aligned} \tag{2}$$

The air-water stress is then calculated from a bulk formula:

$$\vec{\tau}_{\text{air-water}} = \rho_{\text{air}} C_d |\vec{u}_s| \vec{u}_s \tag{3}$$

where $\rho_{\text{air}} = 1.25$ kg m^{-3} is the air density and $C_d = 0.00125$ is the drag coefficient.

[10] The ice-water stress is computed by using daily sea-ice motion vectors gridded to a 25-km resolution [*Fowler*, 2003]. The ice motion data were derived from using satellite [Scanning Multichannel Microwave Radiometer (SMMR), Special Sensor Microwave Imager (SSMI), and Advanced Very High Resolution Radiometer (AVHRR)] and buoy observations. Again, we have followed the AOMIP procedure for the calculation of the ice-water stress:

$$\vec{\tau}_{\text{ice-water}} = \rho_{\text{water}} C_{iw} |\left(\vec{u}_{\text{ice}} - \vec{u}_{\text{ocean}}\right)| \left(\vec{u}_{\text{ice}} - \vec{u}_{\text{ocean}}\right) \tag{4}$$

where ρ_{water} is the water density, $C_{iw} = 0.0055$ is the ice-water drag coefficient, $\vec{u}_{\text{ice}}$ is the ice motion vector from *Fowler* [2003], and $\vec{u}_{\text{ocean}}$ is the upper layer ocean current velocity for which the Ekman velocity $\vec{u}_{\text{Ekman}}$ is used. Although geostrophic velocity is usually considered to be 1 order of magnitude smaller than ice drifting speed, we must point out that it can be large along the coast, in fronts, and in Fram Strait. In these regions, neglecting the geostrophic velocity can induce considerable errors and our calculation can be biased.

[11] With all those data, we can calculate the Ekman layer velocity by using the classic Ekman layer equation [e.g., *Pond and Pickard*, 1983]:

$$-fv_{\text{Ekman}} = \frac{\tau^x}{\rho D_E} \quad \text{and} \quad fu_{\text{Ekman}} = \frac{\tau^y}{\rho D_E} \tag{5}$$

where $D_E = 20$ m is the Ekman layer depth which according to observation is about 18–20 m in the Arctic Ocean [*Hunkins*, 1966]. The Ekman velocity (u_{Ekman}, v_{Ekman}) in equation (5) is the vertically averaged velocity within the Ekman layer. The upwelling and downwelling velocity can be computed from the divergence of the Ekman layer transport, i.e.,

$$w = \nabla \cdot \left(D_E \vec{u}_{\text{Ekman}}\right) \tag{6}$$

The basin-wide and daily upwelling field for a 4-year period from 1995 to 1998 has been computed according to equation (6). The monthly upwelling data are then compiled by using the daily product.

4. Salinity Variations in the Beaufort Sea as Influenced by Ekman Transport and Pumping

[12] We will examine the differences in the salinity distributions between August and December in this section based on the salinity data shown in Figures 2 and 3. The sea-ice motion between December 1995 and August 1998 is shown in Figure 4. In all 3 years, the sea-ice motion vectors in December were dominated by an anticyclonic gyre pattern in the Arctic. The ice velocity was particularly strong in the Beaufort Sea, especially along the southern boundary off Alaska and Canada. This anticyclonic ice motion starts typically in late September or early October, and lasts until the late winter or early spring, for example, April. There are considerable interannual differences during these 3 years. For instance, the transpolar drift, directed from Chukchi and East Siberian Seas toward Fram Strait, was considerably stronger in December 1995 than in other years. The center of the anticyclonic gyre was displaced toward the Siberian Sea in 1997. During the month of August, the pattern of anticyclonic ice motion was absent in all 3 years. In general, the ice drift velocity in the summer months is much weaker, and particularly so in the Beaufort Sea. The geostrophic wind, as shown in Figure 5, was also anticyclonic in the Beaufort Sea in December. There was a considerable similarity between the geostrophic wind and sea-ice drift. For instance, the center of the anticyclonic wind in December 1997 was located further toward the Siberian coast, just like the sea-ice motion. The wind

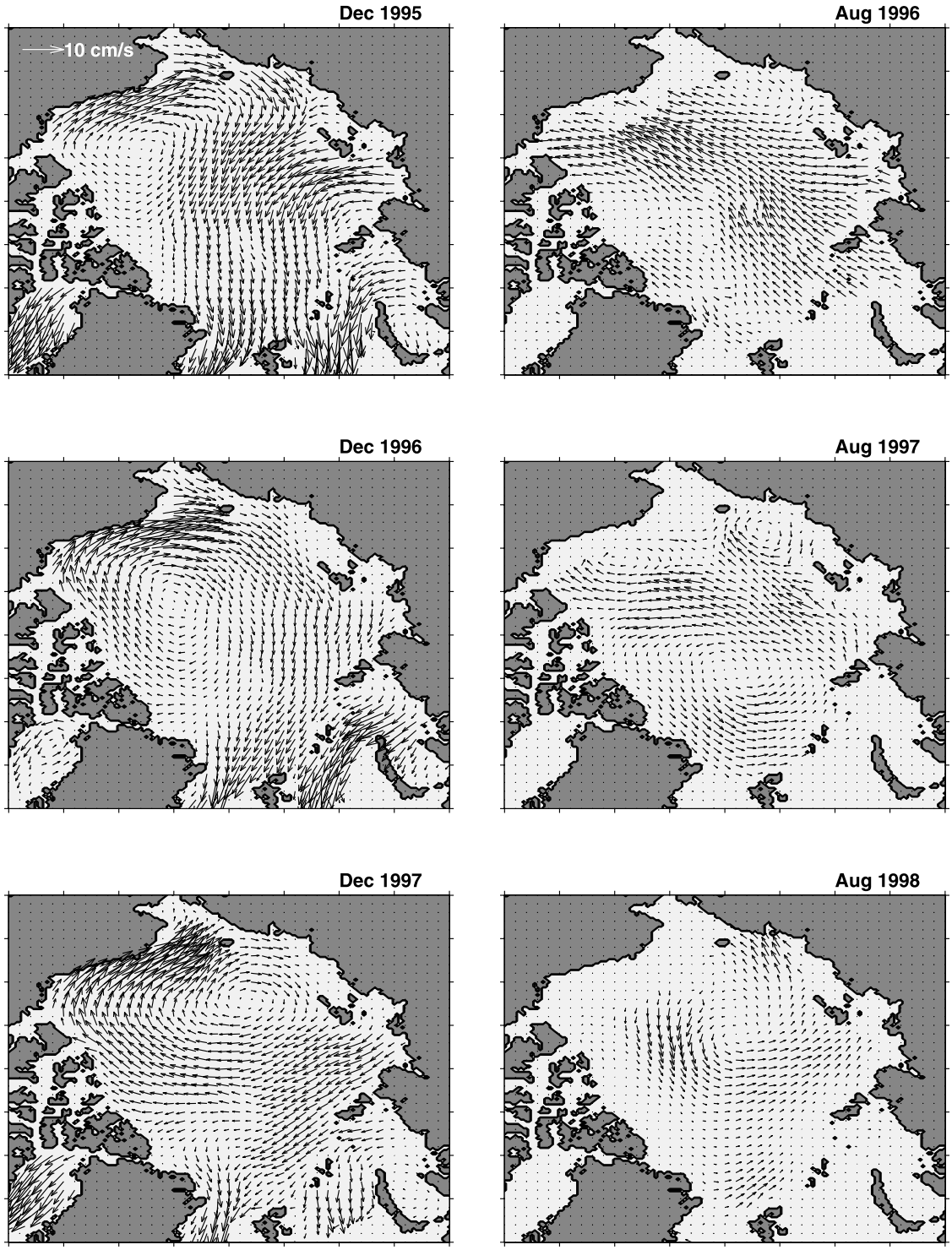

Figure 4. Sea-ice motion vectors for December (left) and August (right) between 1995 and 1998. Note that there was a strong anticyclonic ice motion in all three winter seasons.

coming from Siberian Sea and going toward the Fram Strait was greater in December 1995 than other years. Such a similarity is expected since the sea-ice drift is forced primarily by wind stress. In fact, *Thorndike and Colony* [1982] and *Colony and Thorndike* [1984] showed that the ice velocity can be inferred from the geostrophic wind if a small turning angle is taken into account. To partition the ice-water and air-water stresses, we have used the sea-ice concentration as shown in Figure 6. In all 3 years, the Beaufort Sea was covered almost completely by sea ice in December and had large open-water areas along the southern boundary in August. So the surface stress in the winter months was almost entirely due to the ice motion. Direct wind stress forcing is important in the coastal areas in the

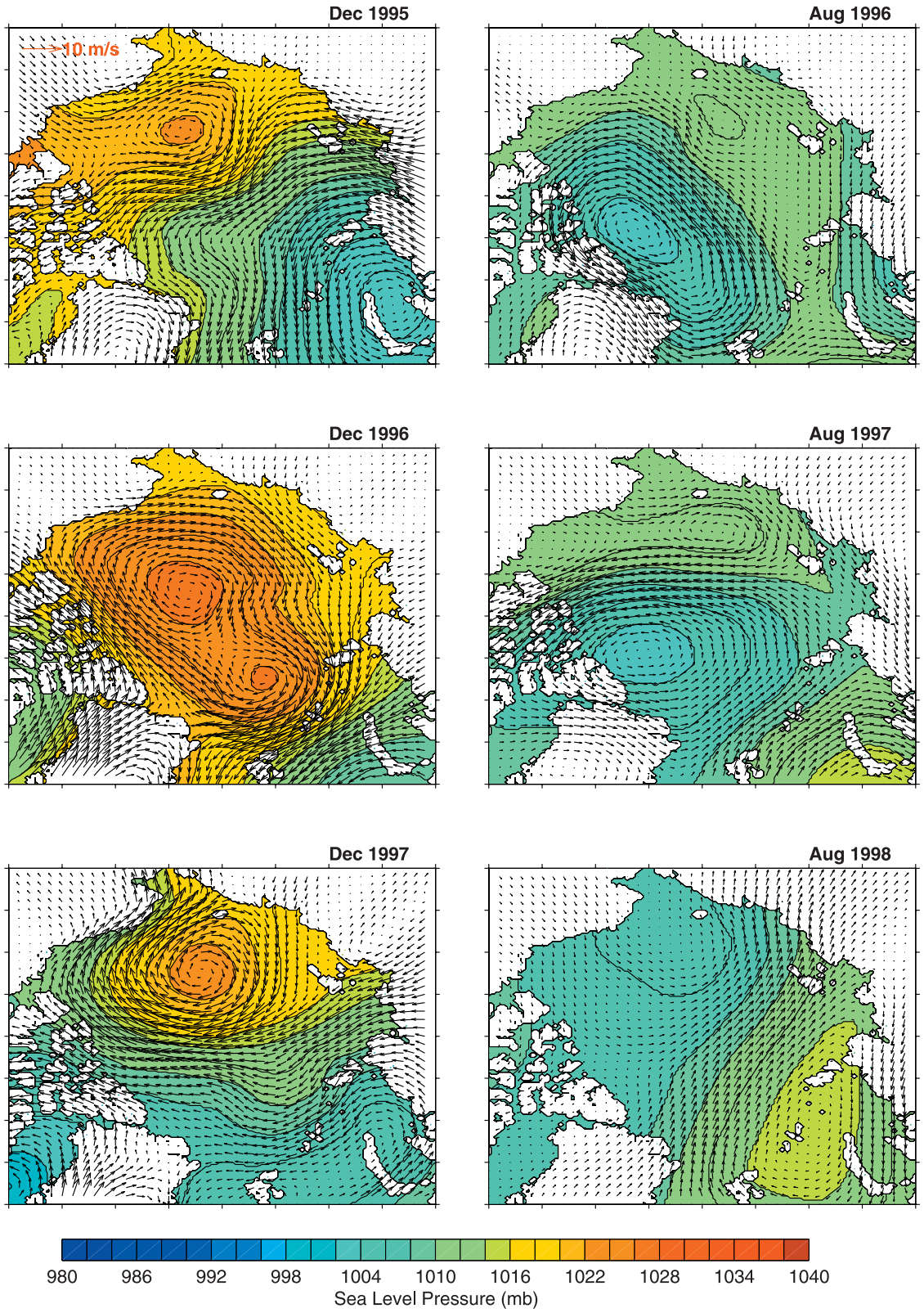

Figure 5. Sea-level pressure (SLP) and surface geostrophic wind vectors for the same months shown in Figure 4.

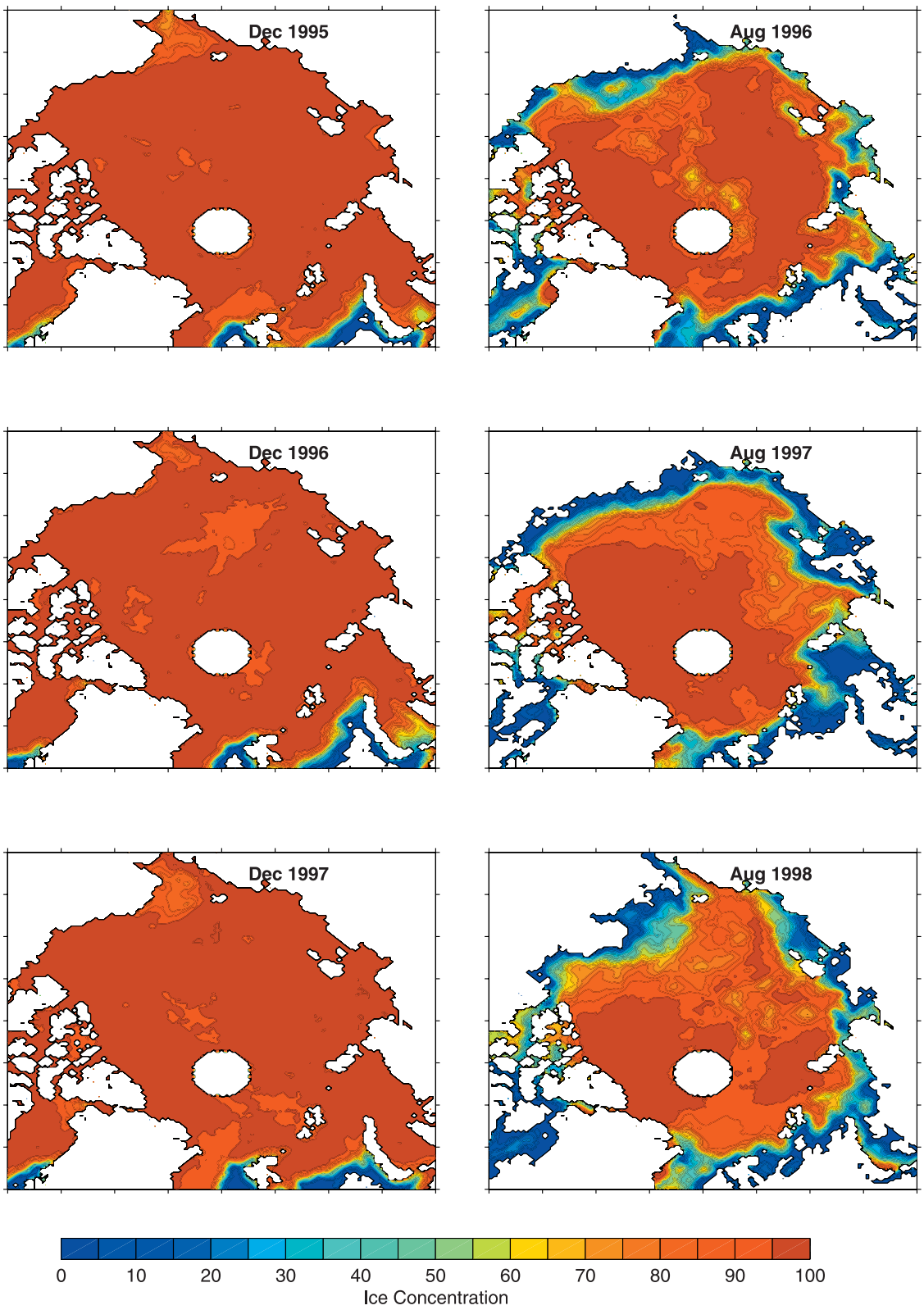

Figure 6. Sea-ice concentrations for the same months shown in Figure 4.

summer. With the forcing fields shown in Figures 4–6, the Ekman transport over the whole model domain has been calculated. But in order to focus on changes in the IOEB areas, we will show results within the black box in Figure 1.

[13] The Ekman velocity field calculated from equation (5) is shown in Figure 7. Driven by the strongly anticyclonic stress vector induced by the ice motion, the Ekman velocity in December was directed offshore from the Alaskan and

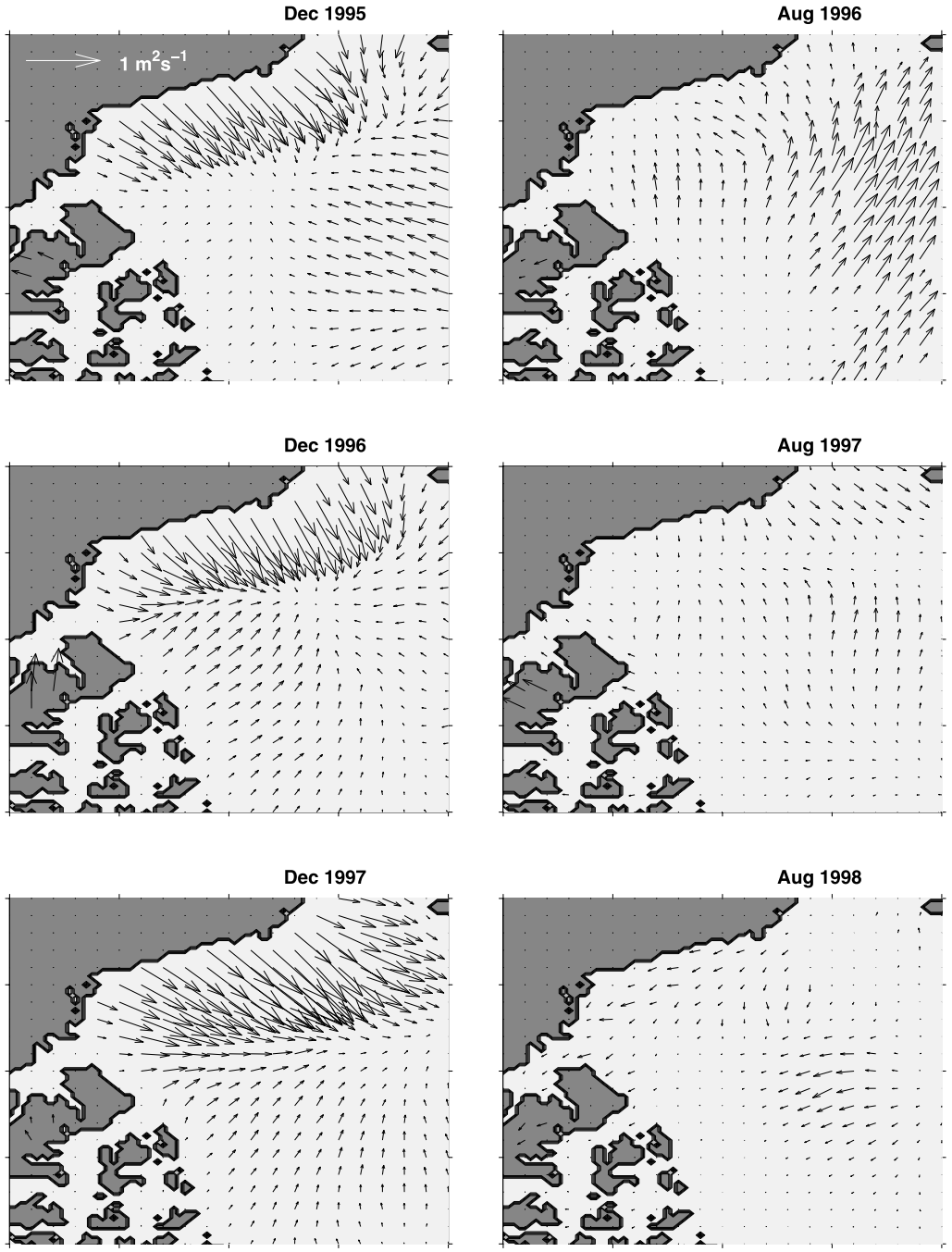

Figure 7. Ekman transport vectors calculated by using equation (5) for the area shown by the black box in Figure 1.

Canadian coast. This resulted in strong upwelling along the boundary and downwelling in the interior Beaufort Sea in the winter season (left panels in Figure 8). Along the boundary, the upwelling velocity was greater than 25 cm/day. The downwelling occurred in a broad area just off the coastal upwelling zone. In August, the Ekman transport was very weak in all 3 years, and there was no coherent similarity among them (right panels in Figure 7). The upwelling and downwelling were also weak except in August 1996 when moderate upwelling was seen in areas near the IOEB buoys (right panels in Figure 8).

[14] How did the horizontal Ekman transport and upwelling/downwelling field relate to the peculiar seasonal variations of salinity shown in Figures 2 and 3? In the Arctic Ocean, the hydrographic structure is quite unique [*Aagaard et al.*, 1981]. Within the upper layer of about 100 or 200 m, the water is well stratified with the presence of a thin mixed layer, a shallow halocline, and a thermocline. The roles of Ekman horizontal advection and vertical pumping can be very different for salinity changes in different depths. The salinity data collected at the depth of 8 m [*Comiso et al.*, 2003, Figure 14] reflected the change that occurred within

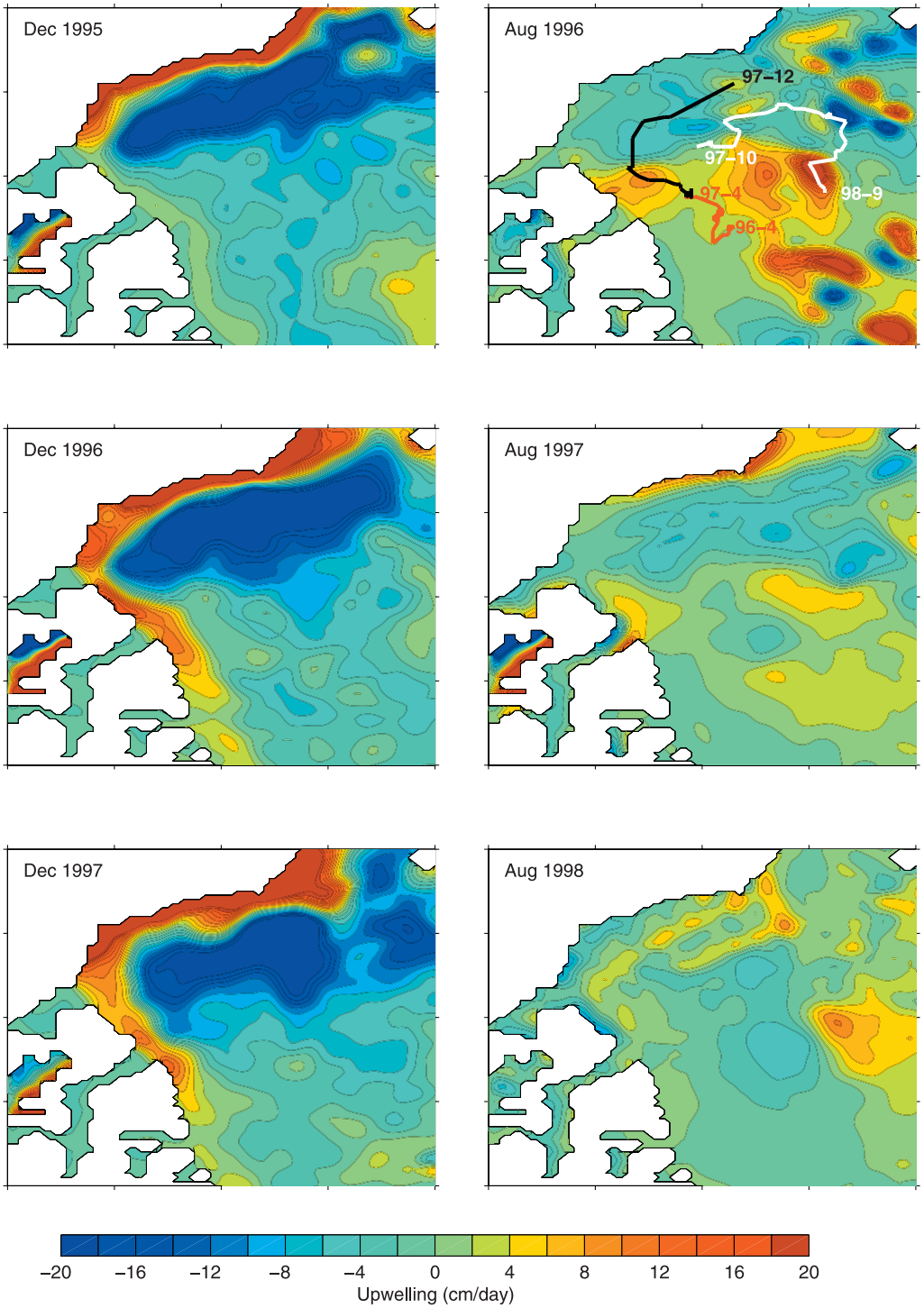

Figure 8. Upwelling and downwelling velocity due to the divergence of the Ekman transport shown in Figure 7.

the surface mixed layer and Ekman layer which has a thickness of about 18 m in the Arctic Ocean [*Hunkins*, 1966]. The salinity in this depth is expected to be directly affected mostly by surface flux of freshwater. Yet the seasonal changes of the salinity, as observed by the Beaufort IOEBs, were similar to that in the deeper layers, i.e., higher salinity in summer months than in the winter months [*Comiso et al.*, 2003]. A downwelling flux would tend to push the mixed layer downward but does not directly affect the water property in the mixed layer (an upwelling does). So the horizontal Ekman advection is expected to play a more direct role than the Ekman pumping at the 8-m depth. The salinity in the surface layer is typically low along the coast in the summer months because of the accumulation of

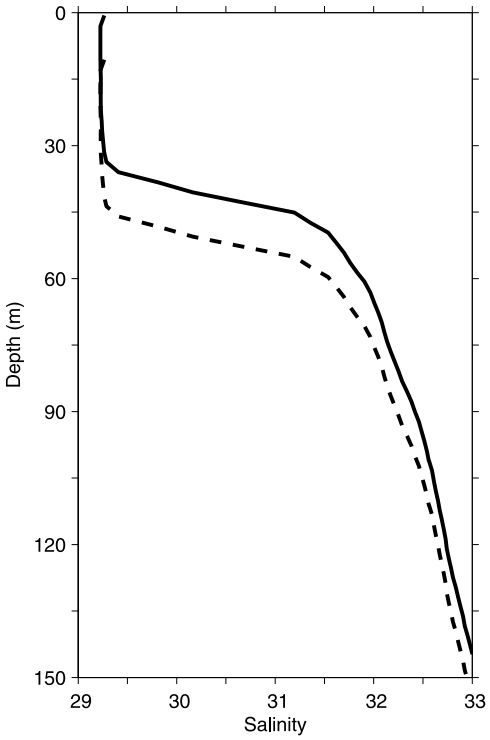

Figure 9. Salinity profile taken in April 1997 when the buoy was refurbished (solid line). Dashed line would be the salinity profile if the downwelling pushed the mixed layer, halocline, and thermocline downward for 10 m. Note that the salinity at all depths below the mixed layer would be lower because of this downward shift.

runoff and melting of ice as the PHC climatology shows [*Steele et al.*, 2000]. When the anticyclonic ice motion and surface wind intensify in the fall and early winter, the low-salinity coastal water would be advected offshore by Ekman currents (left panels in Figure 7). The brine rejection in the winter months, on the other hand, will tend to increase the salinity in the mixed layer. It is likely that the Ekman advection plays a more important role in regions where buoys were located. In such a scenario, the salinity would become lower in the winter because of the offshore Ekman transport of low-salinity coastal waters.

[15] Salinity that was measured at 45-m depth or deeper is affected directly by the Ekman pumping. Two CTD stations were made during the buoy refurbishments, one in April 1996 and the other in April 1997. The T and S profiles in the upper 150 m from these two CTD stations were shown by *Comiso et al.* [2003]. The data were collected when the IOEB buoys were refurbished. The mixed layer depth in both years was about 30–40 m [*Comiso et al., 2003*, Figure 13]. Beneath the mixed layer and to the depth of about 80 m was the Beaufort Sea halocline. In the April 1997 profile, the salinity changed from about 29.25 psu at 35 m to 32 psu at 80 m, a jump of 2.75 PSU over 45 m in depth (Figure 9). The change in April 1996 was smaller, about 1.5 psu, over the same depth range. Because of this strong vertical gradient, the salinity in the upper layer is very sensitive to changes of vertical velocity.

[16] The intensified winter/fall Ekman pumping in the southern Beaufort Sea would result in the deepening of the mixed layer and halocline. A 4-year averaged (1995–1998) monthly distribution of the upwelling field is shown in Figure 10 to describe the seasonal variations over the whole 12 months. Assuming a modest downwelling rate of 10 cm/day for the 4-month period from September to December, the halocline would be pushed down by about 12 m. This would push the mixed layer water to the mean depth of upper halocline layer. In the CTD salinity profile taken in April 1997, the salinity at 35-m depth was about 29.3 psu and at 45 m was about 31.2 psu. If that represents the predownwelling salinity profile and if the halocline were pushed downward by 10 m from September to December, the salinity at 45 m would be reduced by 1.9 psu. Similar estimates would suggest a reduction of salinity of 1 psu at 65 or 76 m. This is quite consistent with a 1-psu change between January and August of 1998 (Figure 3). Figure 9 uses the salinity profile taken in April 1997 to schematize the effect of downwelling on the salinity profile. The solid line is the vertical profile of the salinity in April of 1997 when a CTD station was made during the buoy refurbishment. The dashed line would be the salinity profile if the mixed layer and the halocline were pushed downward by 10 m.

[17] What contribution does the non-Ekman velocity, especially the geostrophic velocity, make in the subsurface layer? The geostrophic velocity in the upper Beaufort Sea is about 1–2 cm/s as inferred from hydrography or from general circulation models and flows anticyclonically around the Beaufort Sea freshwater dome [e.g., *Proshutinsky et al.*, 2004], since the velocity is nearly parallel to the salinity contours because of the fact that the density field in the Arctic is nearly dominated by salinity and to the fact that the salinity structure in Beaufort Sea is dominated by the freshwater dome in association with the Beaufort Gyre as clearly shown in the PHC climatology [*Steele et al.*, 2000]. The salinity gradient along the streamlines of geostrophic velocity is usually small. Here we will examine the 100-m depth change. We take the extreme case by using the maximum salinity difference across the gyre between the center of the dome and the salinity in the southern boundary of Beaufort Gyre. The PHC at 100 m shows about 0.2–0.3 psu (the along streamline salinity difference, which is more relevant here, is much smaller). We also use 500 km for the radius of the gyre and 2 cm/s for geostrophic velocity. The scale of salinity advection, $Ug\Delta S/\Delta L$, is about 8×10^{-9} psu/s, if we assume the upwelling velocity to be 10 cm/day and the salinity difference between surface and 100 m, based on Figure 9, to be 3 psu. The estimate of downwelling's contribution, $W[\Delta S]/D$, is about 3.5×10^{-8} psu/s. So the vertical advection would still be larger than, or at least comparable to, the geostrophic advection. We like to caution here that the use of the long-term climatology could cause a bias in our estimate, and that the actual horizontal ΔS and Ug could be different than what were used here.

[18] We would like to emphasize here that seasonal changes of Ekman transport and upwelling/downwelling do not necessarily alter the freshwater content in the Beaufort Sea. They merely redistribute the water masses within the

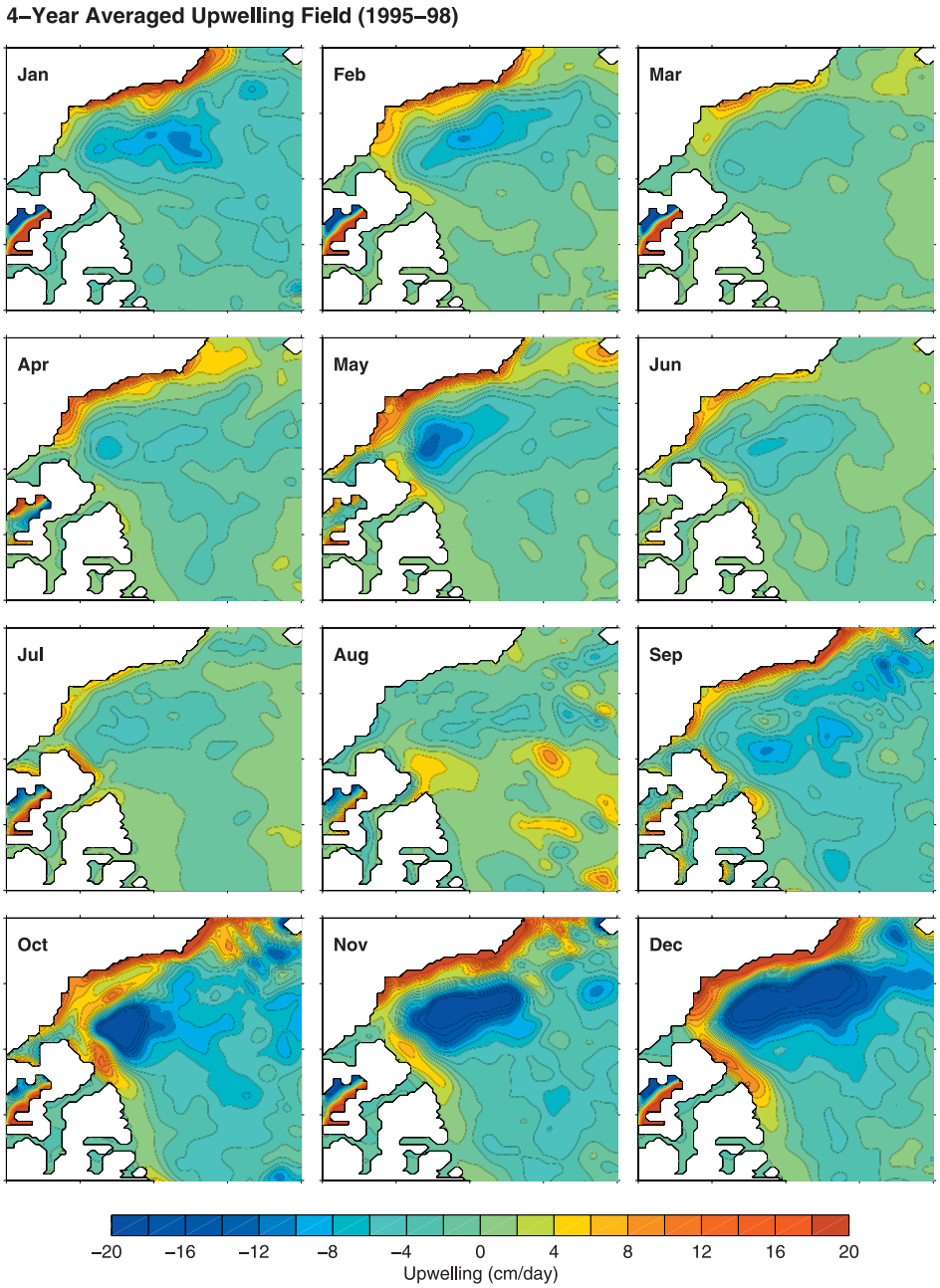

Figure 10. Monthly upwelling field averaged over a 4-year period from January 1995 to December 1998.

area. The variability of freshwater content in the Beaufort Sea is associated with interbasin exchanges [*Hakkinen and Proshutinsky*, 2004], or with external forcing mechanisms, such as river runoff. Indirectly, however, upwelling and downwelling may affect sea-ice freezing and melting cycle through their role in the heat advection. How much this seasonal variation affects the total heat content in the Arctic mixed layer remains to be studied.

[19] It is interesting to note that the type of seasonal variability that is shown in Figures 2 and 3 is different from the climatologic data that were recently produced by *Steele et al.* [2001]. The salinity over the whole Beaufort Sea in either the mixed layer or the halocline-thermocline layer in the PHC climatology is lower in the summer and higher in the winter, the opposite to the IOEB data. There are several factors that may explain this discrepancy. First, the IOEB buoys were located in a narrow region where the contribution from the Ekman transport and upwelling is large. Away from this region, the salinity variability could be affected more directly by freshwater flux, and thus the seasonal change of the salinity could be very different. Because of insufficient data, the discrepancy of the salinity variability in the IOEB region from that of the salinity climatology could not be unambiguously resolved. It is worth noting, however, that interannual and decadal changes in the atmosphere, sea-ice, and ocean circulation have been observed [e.g., *Thompson*

and Wallace, 1998; *Walsh et al.*, 1996; *Proshutinsky and Johnson*, 1987; *Johnson et al.*, 1999; *Rigor et al.*, 2000; *Dickson et al.*, 2000]. The Ekman layer dynamics are forced by the atmosphere and sea ice. So the environmental changes that have taken place in the Arctic will undoubtedly affect the upwelling and downwelling field. The IOEB buoys could have measured only a particular phase of the long-term climate variations while the PHC climatology is the averaged product over many decades. In this sense, the results from this paper are useful in that it may highlight a phenomenon that is not captured by the PHC climatology, which is not really a continuous and spatially detailed record of Arctic Ocean climatology. The impact of long-term climate change on the upwelling field would also be of interest but is not within the scope of this study.

5. Summary

[20] We have used the daily products of sea-ice motion, ice concentration, and surface geostrophic wind to study the upwelling field in the Beaufort Sea in 1996–1998. Because of a strong anticyclonic sea-ice motion pattern that developed in the fall and winter seasons, the Ekman transport was directed away from the southern Beaufort Sea boundary. This resulted in a strong upwelling along the Alaskan and Canadian coast and downwelling in the interior Beaufort Sea. The Ekman transport and upwelling redistributed water masses and resulted in lower salinity in the upper Beaufort Sea away from the boundary. In the summer season, both wind and ice motion patterns are very different, and so the strong downwelling seen in the winter months is absent. Instead, a weak upwelling was shown in the interior Beaufort Sea near the buoy locations. We suggest here that this process explains the unexpected seasonal variability of salinity in the upper Beaufort Sea as observed by IOEB buoys in 1996–1998. Specifically, the offshore Ekman transport brought the low salinity coastal water to the interior in the early winter. This resulted in a fresher mixed layer. The strong downwelling, due to the convergence of the Ekman transport, pushed downward the halocline and thermocline. This would result in a lower salinity at 45, 65, 76, and 165 m where the IOEB salinity sensors were located. We must add a word of caution here about the possibility that the lateral advection may have played an important role, although our scaling analysis indicates that its contribution is smaller than the vertical one. The lateral salinity gradient can be much larger than that derived from the climatology, and associated eddy fluxes can be large. A more comprehensive observational effort or an eddy-resolving modeling study may help to make a more accurate assessment of the relative role of lateral advection.

[21] **Acknowledgements.** This study has been supported by the NSF Office of Polar Program (grant OPP0424074) and by NASA Cryospheric Science Program (grant NNG04GP34G). Discussion with Andrey Proshutinsky has been particularly beneficial. Susumu Honjo and Rick Krishfield have made their IOEB data available to our study.

References

Aagaard, K., L. K. Coachman, and E. Carmack (1981), On the halocline of the Arctic Ocean, *Deep Sea Res., Part A*, *28*, 529–545.

Colony, R., and A. S. Thorndike (1984), An estimate of the mean field of sea ice motion, *J. Geophys. Res.*, *99*, 10,623–10,629.

Comiso, J. C. (1995), Remote sensing of the Arctic, in *Arctic Oceanography: Marginal Ice Zones and Continental Shelves, Coastal Estuarine Study*, edited by W. Smith and J. Grebmeier, pp. 1–50, AGU, Washington, D. C.

Comiso, J. C., J. Yang, S. Honjo, and R. A. Krishfield (2003), Detection of change in the Arctic using satellite and in situ data, *J. Geophys. Res.*, *108*(C12), 3384, doi:10.1029/2002JC001347.

Dickson, R. R., T. J. Osborn, J. W. Hurrell, J. Meincke, J. Blindheim, B. Aadlandsvik, T. Vinje, G. Alekseev, and W. Maslowski (2000), The Arctic Ocean response to the North Atlantic Oscillation, *J. Clim.*, *13*, 2671–2696.

Fowler, C. (2003), Polar Pathfinder Daily 25km EASE-Grid Sea Ice Motion Vectors, National Snow and Ice Data Center, Boulder, CO, Digital Media. (http://nsidc.org)

Hakkinen, S., and A. Proshutinsky (2004), Freshwater content variability in the Arctic Ocean, *J. Geophys. Res.*, *109*, C03051, doi:10.1029/2003JC001940.

Honjo, S., T. Takizawa, R. Krishfield, J. Kemp, and K. Hatakeyama (1995), Drifting buoys make discoveries about interactive processes in the Arctic Ocean, *Eos Trans. AGU*, *76*(21), 209215, 219.

Hunkins, K. (1966), Ekman drift currents in the Arctic Ocean, *Deep Sea Res.*, *13*, 607–620.

Johnson, M. A., A. Y. Proshutinsky, and I. V. Polyakov (1999), Atmospheric patterns forcing two regimes of Arctic circulation: A return to anticyclonic condition?, *Geophys. Res. Lett.*, *26*, 1621–1624.

Krishfield, R. (1999), Ice-Ocean Environmental Buoy Program: Archived Data Processing and Graphical Results from April 1992 through November 1998, WHOI Technical Report, WHOI-99-12.

Pond, S., and G. Pickard (1983), *Introductory Dynamical Oceanography*, pp. 329, Elsevier, New York.

Proshutinsky, A. Y., and M. A. Johnson (1987), Two circulation regimes of the wind-driven Arctic Ocean, *J. Geophys. Res.*, *102*, 12,493–12,514.

Proshutinsky, A. Y., et al. (2001), Multinational effort studies differences among Arctic Ocean models, *Eos Trans. AGU*, *82*, 637–644.

Proshutinsky, A., R. Krishfield, E. Carmack, F. McLaughlin, S. Zimmerman, K. Shimada, and M. Itoh (2004), Annual freshwater and heat content from 2003–2004: First results from the Beaufort Gyre Observing System, *Eos Trans. AGU*, *85*(47), Fall Meet. Suppl.

Rigor, I. (2002), *IABP Drifting Buoy, Pressure, Temperature, Position, and Interpolated Ice Velocity*, Compiled by the Polar Science Center, Applied Physics Laboratory, University of Washington, Seattle, in association with NSIDC, National Snow and Ice Data Center, Boulder, CO, Digital medi.

Rigor, I. G., R. Colony, and S. Martin (2000), Variations in surface air temperature observations in the Arctic, 1979–97, *J. Clim.*, *13*, 896–914.

Steele, M., R. Morley, and W. Ermold (2000), PHC: A global hydrography with a high-quality Arctic Ocean, *J. Clim.*, *14*, 2079–2087.

Thorndike, A. S., and R. Colony (1982), Sea ice motion in response to geostrophic winds, *J. Geophys. Res.*, *87*, 5845–5852.

Thompson, D. W. J., and J. M. Wallace (1998), The Arctic Oscillation signature in wintertime geopotential height and temperature fields, *Geophys. Res. Lett.*, *25*, 1297–2000.

Walsh, J. E., W. L. Chapman, and T. L. Shy (1996), Recent decrease of sea level pressure in the central Arctic, *J. Clim.*, *9*, 480–486.

Yang, J., J. Comiso, D. Walsh, R. Krishfield, and S. Honjo (2004), Storm-driven mixing and potential impact on the Arctic Ocean, *J. Geophys. Res.*, *109*, C04008, doi:10.1029/2001JC001248.

J. C. Comiso, Laboratory for Hydrospheric and Biospheric Sciences, NASA Goddard Space Flight Center, Greenbelt, MD 20771, USA. (josefino.c.comiso@nasa.gov)

J. Yang, Department of Physical Oceanography, Woods Hole Oceanographic Institution, Woods Hole, MA 02543, USA. (jyang@whoi.edu)